

Nanocrystal shape and nanojunction effects on electron transport in nanocrystal-assembled bulks

*Shao-Chien Chiu,^a Jia-Sin Jhang,^a Yen-Fu Lin,^a Shih-Ying-Hsu,^a Jiye Fang,^b and Wen-Bin Jian^{*a}*

^aDepartment of Electrophysics, National Chiao Tung University, Hsinchu 30010, Taiwan, ROC

^bDepartment of Chemistry, State University of New York at Binghamton, Binghamton, New
York 13902-6000, USA

*wbjian@mail.nctu.edu.tw

This SI file contains more details about I. Experiments and Device Information, II. Particle Size Distribution, III. Capping Agents, IV. Inter-Particle Capacitances, V. Devices of Metallic Features, VI. Fitting to Figure 3(a), VII. Fitting Parameters. VIII. Statistic on Arrangements between Neighboring Nanocrystals.

I. Experiments and Device Information

The scheme of the fabrication process of a small piece of a PbSe NC-assembled bulk is presented

in Fig. S1. Through the first-time electron-beam patterning, two Pt electrodes with a special shape (see **Figure S1(a)**) were deposited on Si wafer which was capped with a 300-nm thick SiO₂ layer. The trench of ~25 μm in length, ~1 μm in width, and ~20 nm in depth is formed between a pair of Pt electrodes. Each Pt electrode is in connection with a larger Ti/Au electrode patterned by photolithography with thermal evaporation. **Figure S1(b)** presents a spin-coated PMMA layer (in light blue) with an opening window on top of the trench and the Pt electrodes. The PMMA window was opened by the second-time electron-beam patterning. PbSe NC suspension was drop-casted on surface of the PMMA protected device (**Figure S1(c)**). After the device substrate was dried in air, PbSe NC self-assembled and formed a thin film on the PMMA surface. In particular, a piece of NC-assembled bulk was molded on the opening-window area. The PMMA thin film was removed by immersing the device substrate in acetone for 1 h. After removing the PMMA and excess NCs, only the NC-assembled bulk on the opening-window area remained on surface (**Figure S1(d)**). Then, the device substrate was dried by nitrogen gas flow.

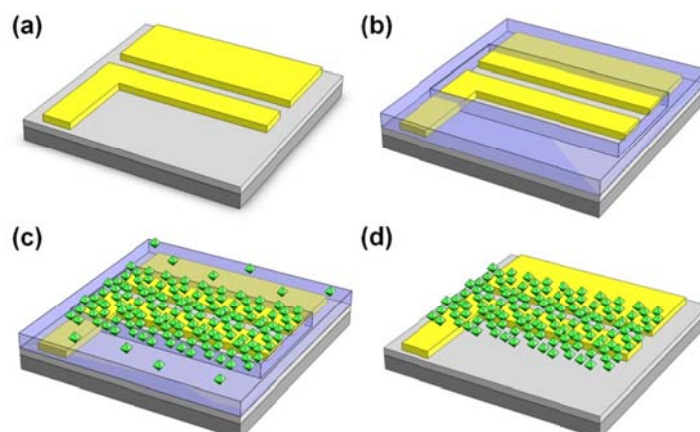


Figure S1. Fabrication scheme of a PbSe NC-assembled bulk.

Information of several typical devices is listed in **Table S1**. It is noted that the effective conducting volume of the NC-assembled bulk is the volume on the trench area rather than on the opening-window area.

	Duration (min)	$L/W/T$ (μm)	R_{RT} (Ω)	ρ_{RT} ($\Omega \text{ cm}$)
NC225-1	10	2.0/6.3/1.0	1.64×10^9	5.16×10^5
NC225-2	10	1.0/25.0/1.0	1.59×10^8	3.97×10^5
NC225-3	10	1.0/25.0/1.0	5.94×10^7	1.49×10^5
NC225-4	30	1.0/25.0/1.0	9.38×10^6	2.34×10^4
NC225-5	30	2.0/6.3/1.0	3.70×10^7	1.16×10^4
NC250-1	360	1.0/25.0/1.0	6.41×10^4	1.60×10^2
NC250-2	10	3.0/2.8/1.0	7.72×10^4	7.20×10^0
NC250-3	360	1.0/25.0/1.0	6.89×10^5	1.72×10^3

NC250-4	10	1.0/25.0/1.0	4.26×10^4	1.07×10^2
NC250-5	10	1.0/25.0/1.0	3.54×10^4	8.86×10^1
NC250-6	10	1.0/25.0/1.0	3.88×10^5	9.69×10^2
NC275-1	60	1.0/25.0/1.0	6.24×10^2	1.56×10^0

Table S1: Device information of annealing time, dimensions of the effective conducting volume, resistance R_{RT} and resistivity ρ_{RT} at room temperature.

II. Particle Size Distribution

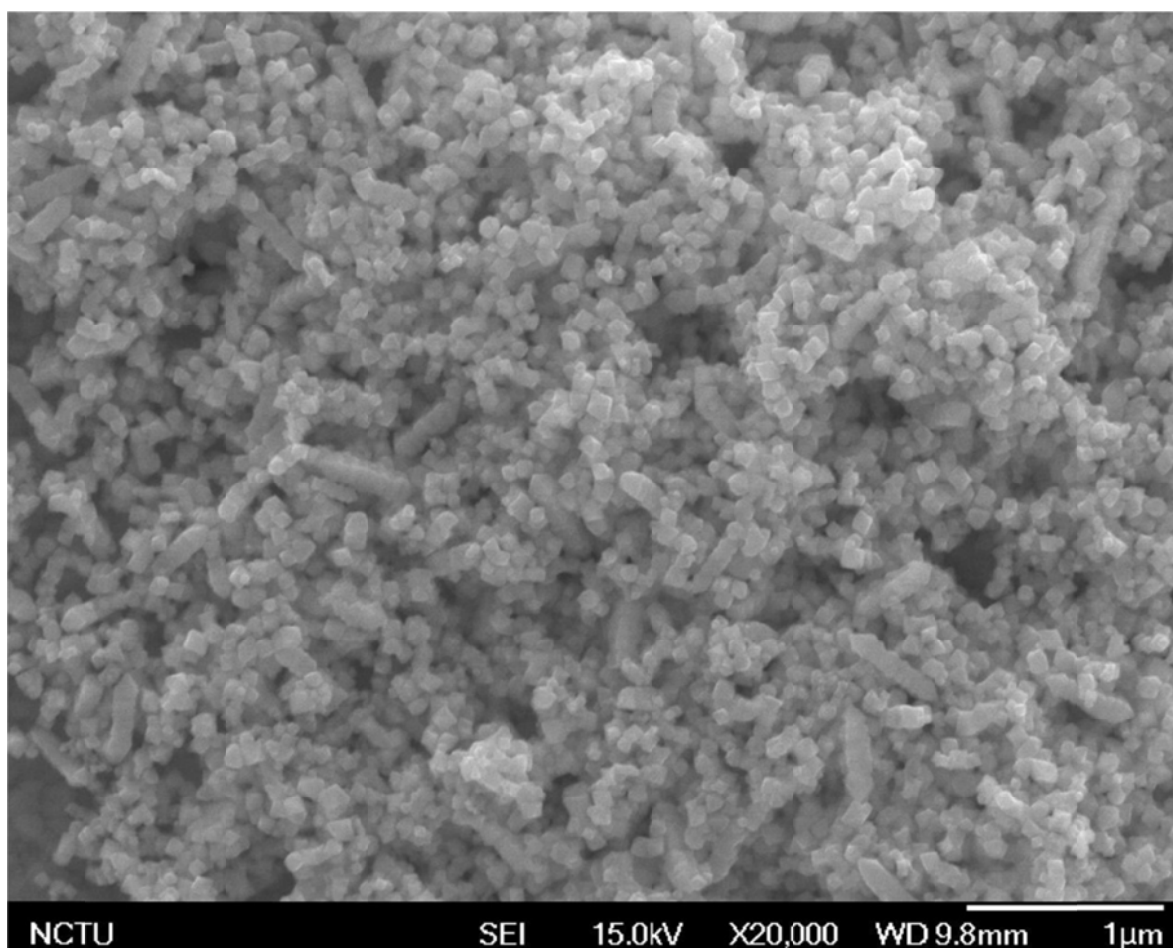


Figure S2. SEM image of the PbSe NCs.

Figure S2 presents a typical SEM image used for estimations of size distribution (see Figure 1(b) in the manuscript) and average size of the PbSe NCs. The average size (D) was statistically estimated to be 122 ± 18 nm. Total count for average size evaluation is 372. The PbSe NCs in the SEM image are the same batch to those used for electrical property measurements.

III. Capping Agents

The capping agents of our PbSe NCs are oleic acids and trioctylphosphine thus the inter-particle distance is controlled by these organic molecules. Considering the interpenetration of oleic acids, the spacing between neighboring QDs is estimated to be about 2 nm.¹

In our experiments, we adopted thermal annealing to reduce the spacing between neighboring nanocrystals. The two organic molecules started to decompose at 200 °C.^{2,3} The decomposition corroborates that a longer time is required for thermal annealing at 225 °C while a shorter time is enough for that at 250 °C. Thus the resistivity of the 250 °C-annealed, NC-assembled bulk is almost irrelevant to the annealing time (see the discussion of **Figure 2(d)** in the manuscript).

IV. Inter-Particle Capacitances

The charging energy of the rather big PbSe NC (~122 in diameter) is too small to be considerable. On the other hand, the thermal fluctuation voltage which is determined by the inter-particle capacitance shall be taken into consideration. Since PbSe single crystal is metallic, the simple parallel plate model was used for evaluation of the inter-particle capacitance between PbSe NCs. From SEM and TEM images, two possible arrangements, face-to-face and edge-to-edge configurations, between NCs are observed and, therefore, the inter-particle capacitances are estimated in **Table S2** according to the expression $C = \epsilon A / d$, where A is the area of the plate on NCs, d is the spacing between NCs, and ϵ is the dielectric constant of the capping agents.

For the face-to-face configuration between two NCs, we take the facet of the octahedral NC (~122 nm in diameter) as the area of the parallel plates. On the other hand, the area of the edge-to-edge configuration between NCs is taken as $\sim 1 \text{ nm}^2$ which will be justified in **Section VI** in this **Supplementary Material**. The thermal fluctuation voltage is calculated from the equation

$$V_T = (k_B T / C)^{1/2}, \text{ where } k_B \text{ is the Boltzmann constant.}$$

	A (nm ²)	d (nm)	ϵ	C (F)	$V_{T, 300\text{ K}}$ (V)
Face-to-face	3222	2	2	$\sim 1 \times 10^{-17}$	~ 0.02
Edge-to-edge	1	2	2	$\sim 1 \times 10^{-20}$	~ 0.64

Table S2: Table of inter-particle capacitances and thermal fluctuation voltages for face-to-face and edge-to-edge arrangements between PbSe octahedral QDs.

V. Devices of Metallic Features

In the manuscript, we describe that the 275 °C-annealed NC-assembled bulk reveals a metallic feature. The temperature dependent resistance of the NC275-1 device can be well described by the expression $R(T) = R_0 + cT$, where $R_0 = 511$ and $c = 0.3$ are two parameters. The positive c value confirms a metallic $R-T$ dependence. **Table S3** gives a comparison of electrical properties between our samples and those reported in the literatures. It is noted that the conductivity of the 275 °C-annealed NC-assembled bulk is smaller than that of single-crystalline film. The problem could be attributed to the estimation of the dimension of our NC-assembled bulk. It is obvious that many holes and voids exist in the NC-assembled bulk so the real dimension shall be much smaller and the conductivity will be higher.

	Conductivity ($\Omega \text{ cm}$) ⁻¹	Transport
225 °C-annealed NC-assembled bulk	$\sim 1 \times 10^{-6}$	semiconductor
250 °C-annealed NC-assembled bulk	$\sim 1 \times 10^{-3}$	semiconductor
275 °C-annealed NC-assembled bulk	~ 1	metal
Polycrystalline film ⁴	5.51×10^{-2}	semiconductor
Single-crystalline film ⁵	$\sim 1 \times 10^2$	metal

Table S3: A comparison of conductivity and transport behavior between our samples, and poly- and single-crystalline films.

VI. Fitting to Figure 3(a)

The equations of $\rho(T) = \rho_0 \exp(T_1 / (T_0 + T))$, $\rho(T) = \rho_1 \exp((T_2 / T)^{1/4})$, $\rho(T) = \rho_2 \exp(E_a / k_B T)$ are used for fittings to the models of the FITC, the Mott's 3D VRH, and the thermal activation, respectively, where ρ_0 , ρ_1 , ρ_2 , T_0 , T_1 , T_2 , and E_a are fitting parameters and k_B is the Boltzmann constant. Data of temperature dependent resistivity in **Figure 3(a)** in the manuscript are fitted by Monte Carlo method and the standard deviations are estimated to be 11, 18, and 647 for models of the FITC, the Mott's 3D VRH, and the thermal activation. Thus, it is clear that the FITC model is the best to analyze the electron transport in the PbSe NC-assembled bulks. In addition, according to the analysis of the electric-field dependent

resistivity (see **Figure 4** in the manuscript), the FITC model depicts in high agreement with the experimental data.

VII. Fitting Parameters

The fitting parameters extracted from the data of $R-T$ dependence of those semiconducting devices are listed in **Table S4**. The estimated junction width w which is less than ~ 2 nm is in line with the spacing between neighboring NCs. In addition, the spacing is in line with the length of capping agents.

	R_0 (Ω)	T_1 (K)	T_0 (K)	T_1/T_0	w (nm)	A (\AA^2)
NC225-1	1.77×10^6	2.46×10^3	71	34.6	2.02	2.33
NC225-2	5.72×10^3	5.29×10^3	228	23.2	1.35	3.35
NC225-3	3.44×10^3	4.95×10^3	226	21.9	1.28	2.96
NC225-4	5.02×10^4	2.49×10^3	182	13.7	0.80	0.93
NC225-5	1.75×10^3	5.05×10^3	234	21.6	1.26	2.98
NC250-1	1.14×10^3	1.77×10^3	134	13.2	0.77	0.64
NC250-2	5.14×10^2	2.29×10^3	163	14.0	0.82	0.88
NC250-3	5.54×10^3	3.03×10^3	270	11.2	0.65	0.93
NC250-4	1.77×10^1	3.84×10^3	277	13.9	0.81	1.45
NC250-5	1.46×10^3	1.56×10^3	172	9.1	0.53	0.39
NC250-6	2.82×10^3	2.82×10^3	188	15.0	0.87	1.16

Table S4: Fitting parameters from $R(T)$ according to the FITC model.

The fitting results indicate a very small junction area A for the edge-to-edge configuration between neighboring NCs. To corroborate the fitting results as well as our previous estimation of inter-particle capacitances, we go back to analyze the sharpness of apexes of the octahedral NCs. **Figure S3** presents several SEM images of apexes on individual PbSe NCs. The curvature on tip of apexes can roughly be decided by a sphere. The average diameter of the tip on apexes is 5.6 ± 0.9 nm. Taking the edge of the junction area as one tenth of the average diameter (0.56 nm), the junction area will be about 30 \AA^2 . This estimated value is still one order of magnitude large than the fitting results shown in **Table S4**. Another possible reason could be due to overestimation of the junction barrier height. We use the ideal junction barrier of 4.56 eV in the calculation. When the junction barrier is, for example, as low as 2 eV due to imaginary forces, the fitting result of the junction area will be larger than 10 \AA^2 . As a result, our fitting results are in line with the real geometry of our system, the NC-assembled bulk.

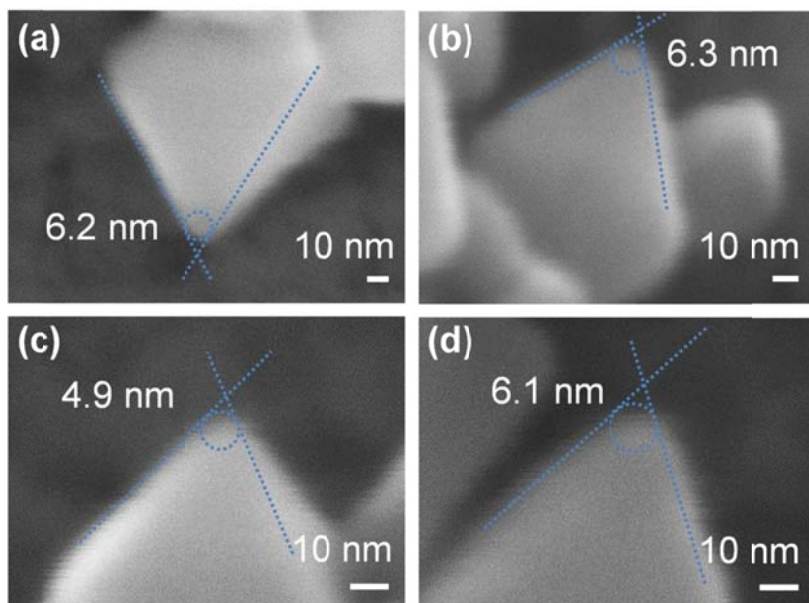


Figure S3. SEM images of individual PbSe NC.

In addition to $R(T)$, we fitted the I-V data according to the equation $I = I_0 \exp\left\{-a(t)\left[\left(V/V'\right)-1\right]^2\right\}$ and obtained the fitting parameter V' of 16.2 V. The FITC model gives the relation $V' = (4V_0(L/D))/e$. If we take L/D as the number of total junctions in the trench (about 10), the ideal V' value shall be $10 \times 4 \times 4.56 = 182.4$. The ideal value is about ten times larger than the fitting result. Such an inconsistency cannot be explained but it exists in previous reports.^{6,7}

VIII. Statistic on Arrangements between Neighboring Nanocrystals.

The SEM images of annealed PbSe NCs show in **Figure S4** were used to estimate the ratio between different types of configurations. The percentage of edge-to-edge and face-to-face configurations are 65.5 and 34.5 percent, respectively. Total count for the estimation of occupation ratio is 61.

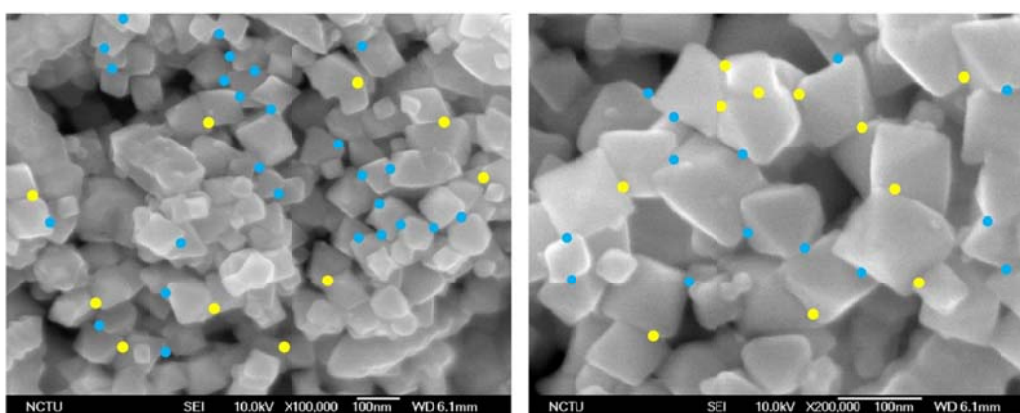


Figure S4. SEM images of the annealed PbSe NCs used to estimate the percentage of NC arrangements.

1. J. S. Steckel, S. Coe-Sullivan, V. Bulović and M. G. Bawendi, *Adv. Mater.*, 2003, **15**, 1862.
2. K. A. S. Fernando, M. J. Smith, B. A. Harruff, W. K. Lewis, E. A. Guliants and C. E. Bunker, *J. Phys. Chem. C*, 2009, **113**, 500.
3. P. I. Archer, P. V. Radovanovic, S. M. Heald and D. R. Gamelin, *J. Am. Chem. Soc.*, 2005,

127, 14479.

4. S. Kumar, Z. H. Khan, M. A. Majeed Khan and M. Husain, *Curr. Appl. Phys.*, 2005, **5**, 561.
5. J. N. Zemel, J. D. Jensen and R. B. Schoolar, *Phys. Rev.*, 1965, **140**, A330.
6. P. Sheng, E. K. Sichel and J. I. Gittleman, *Phys. Rev. Lett.*, 1978, **40**, 1197.
7. Y. H. Lin and J. J. Lin, *J. Appl. Phys.*, 2011, **110**, 064318.